AFRL-AFOSR-JP-TR-2024-0052

Stoichiometric Doping of Copper Sulfide Nanocrystals Assemblies with Tunable Electronic Properties

Huh, Wansoo
Soongsil University Industry-Academic Cooperat
369 Sangdo-ro, Dongjak-gu
Seoul, , 06978
KR

02/21/2024
Final Technical Report

Air Force Research Laboratory
Air Force Office of Scientific Research
Asian Office of Aerospace Research and Development
Unit 45002, APO AP 96338-5002

REPORT DOCUMENTATION PAGE

PLEASE DO NOT RETURN YOUR FORM TO THE ABOVE ORGANIZATION.

1. REPORT DATE	2. REPORT TYPE	3. DATES COVERED	
20240221	Final	START DATE 20200930	END DATE 20230929

4. TITLE AND SUBTITLE
Stoichiometric Doping of Copper Sulfide Nanocrystals Assemblies with Tunable Electronic Properties

5a. CONTRACT NUMBER	5b. GRANT NUMBER	5c. PROGRAM ELEMENT NUMBER
	FA2386-20-1-4088	
5d. PROJECT NUMBER	**5e. TASK NUMBER**	**5f. WORK UNIT NUMBER**

6. AUTHOR(S)
Wansoo Huh

7. PERFORMING ORGANIZATION NAME(S) AND ADDRESS(ES)
Soongsil University Industry-Academic Cooperat
369 Sangdo-ro, Dongjak-gu
Seoul 06978
KR

8. PERFORMING ORGANIZATION REPORT NUMBER

9. SPONSORING/MONITORING AGENCY NAME(S) AND ADDRESS(ES)	10. SPONSOR/MONITOR'S ACRONYM(S)	11. SPONSOR/MONITOR'S REPORT NUMBER(S)
AOARD UNIT 45002 APO AP 96338-5002	AFRL/AFOSR IOA	AFRL-AFOSR-JP-TR-2024-0052

12. DISTRIBUTION/AVAILABILITY STATEMENT
A Distribution Unlimited: PB Public Release

13. SUPPLEMENTARY NOTES

14. ABSTRACT
In this project, we developed a versatile conversion platform that allows delicate control in the atomic stoichiometry for highly coupled Cu2-xS NCs assemblies with tunable electronic properties including the optical properties, charge transport properties, and thermoelectrical properties. The control in the atomic stoichiometry was done through two distinct methods. First, the control was done by directly inserting/extracting copper into/from the assemblies using a solution phase chemical agent. Specifically, the stoichiometry of Cu2-xS NCs assemblies could be controlled from x = 0.1 to 0.9 . With increasing x, we confirmed that the absorbance at near IR regime, electrical conductivity, and Seebeck coefficient changed systematically, leading to the maximal thermoelectric power factor from a film of Cu2-xS NCs at an optimal doping condition yielding x = 0.1. Second, the atomic composition for assemblies of Cu2-xS NC (x = 0.9) could also be controlled by introducing monovalent heterocations (such as lithium or sodium) into the assemblies and reversibly extracting these cations from the assemblies through electrochemical method. The electrochemically controlled uptake and release of the cations for assemblies of Cu2-xS NC allow systematic tuning in the characteristic near-infrared absorbance of the thin-film assemblies based on localized surface plasmon resonance.

15. SUBJECT TERMS

16. SECURITY CLASSIFICATION OF:			17. LIMITATION OF ABSTRACT	18. NUMBER OF PAGES
a. REPORT U	b. ABSTRACT U	c. THIS PAGE U	SAR	13

19a. NAME OF RESPONSIBLE PERSON	19b. PHONE NUMBER *(Include area code)*
TODD RUSHING	315-227-7003

Standard Form 298 (Rev.5/2020)
Prescribed by ANSI Std. Z39.18

Stoichiometric Doping of Copper Sulfide Nanocrystals Assemblies with Tunable Electronic Properties

Wansoo Huh[1] and Moon Sung Kang[2]

[1]Department of Chemical Engineering, Soongsil University, Seoul Korea

[2]Department of Chemical and Biomolecular Engineering, Sogang University, Seoul Korea

Abstract

In this project, we developed a versatile conversion platform that allows delicate control in the atomic stoichiometry for highly coupled $Cu_{2-x}S$ NCs assemblies with tunable electronic properties including the optical properties, charge transport properties, and thermoelectrical properties. The control in the atomic stoichiometry was done through two distinct methods. First, the control was done by directly inserting/extracting copper into/from the assemblies using a solution phase chemical agent. Specifically, the stoichiometry of $Cu_{2-x}S$ NCs assemblies could be controlled from $x = 0.1$ to 0.9 . With increasing x, we confirmed that the absorbance at near IR regime, electrical conductivity, and Seebeck coefficient changed systematically, leading to the maximal thermoelectric power factor from a film of $Cu_{2-x}S$ NCs at an optimal doping condition yielding $x = 0.1$. Second, the atomic composition for assemblies of $Cu_{2-x}S$ NC ($x = 0.9$) could also be controlled by introducing monovalent heterocations (such as lithium or sodium) into the assemblies and reversibly extracting these cations from the assemblies through electrochemical method. The electrochemically controlled uptake and release of the cations for assemblies of $Cu_{2-x}S$ NC allow systematic tuning in the characteristic near-infrared absorbance of the thin-film assemblies based on localized surface plasmon resonance.

"Stoichiometric Doping of Highly Coupled $Cu_{2-x}S$ Nanocrystal Assemblies" *ACS Appl. Mater. Interfaces* 2021, 13, 26330, 10.1021/acsami.1c03853

"Electrochemical Lithium Doping of $Cu_{2-x}S$ Nanocrystal Assemblies for Tuning Their Near Infrared Absorbance" *J. Mater. Chem. C* 2023, 11, 4466, 10.1039/D3TC00076A

A small number of copper escaped from lattice of copper sulfide nanocrystals yields stoichiometric mismatch between copper and sulfide atoms in the material, i.e. $Cu_{2-x}S$ NCs (where x represents the degree of mismatched stoichiometry). Interestingly, this mismatch in stoichiometry leads to generate extra holes in the material, providing it with self-doped *p*-type electronic characteristics. Thus, delicate control in the atomic stoichiometry of the material allows fine tuning in the material characteristics. For examples, localized surface plasmon resonance

(LSPR) effect based on plentiful of free holes of $Cu_{2-x}S$ NCs can be varied by changing x. Photoluminescence of $Cu_{2-x}S$ NCs can also be varied upon changing x. Perhaps, the catalytic effect of the material, which is often employed for photocatalytic hydrogen evolution reaction and carbon dioxide reduction reaction, should also vary with x. Along this line, methods to control x for $Cu_{2-x}S$ NCs has been developed, which is done in solution phase (one can exploit metal complex solution to introduce Cu ions into the material or extract Cu ions from the material) and the as-tuned properties of $Cu_{2-x}S$ NCs in solution has been demonstrated.

When exploiting NCs in electronic devices or in electrochemical systems, however, they must form assemblies and be deposited into thin-films. Under such circumstance, the physical characteristics of NCs forming assemblies are not only determined by the intrinsic properties of NC alone but also by how the materials are coupled electronically with each other in assemblies. This can primarily be achieved by engineering ligands attached onto NCs. Typically, short thiols, short amines, thiocyanides, and halides have been employed for such purpose for assemblies of $Cu_{2-x}S$ NCs. However, up to now, the influence of the atomic composition or x on the physical properties of such highly coupled $Cu_{2-x}S$ NC assemblies has been rarely studied (the studies on the coupling in the NC assemblies and on stoichiometry effect on individual NC properties have been studied separately). We emphasize that these highly coupled $Cu_{2-x}S$ NCs are unique nanostructure systems whose charge density can be controlled with post treatment varying x (which we refer as *stoichiometric doping*) without altering the morphology/ordering of the assembly. Thus, a versatile platform to explore the electronic properties of nanostructure semiconductors can be provided.

Throughout this research project, we developed a versatile conversion platform that allows delicate control in the atomic stoichiometry for *highly coupled $Cu_{2-x}S$ NCs assemblies* that can be readily integrated into electronic devices. Using the platform, we investigated the fundamental electronic properties of the semiconductor nanocrystal assemblies, including the optical properties, charge transport properties, and thermoelectrical properties.

One way to change the atomic stoichiometry of $Cu_{2-x}S$ NCs is to vary the ratio of copper and sulfur precursors included in the crystal growth level or to control the reactivity of these precursors by adjusting the surface ligands that is dynamically absorbed on the crystal surface during the growth. The method is simple, yet acquiring on-demand control on the atomic stoichiometry from such method is not trivial, considering the experimental uncertainties included in the crystal growth. The atomic stoichiometry of $Cu_{2-x}S$ NCs can be also controlled by the post-treatment after the synthesis and or even after thin-film deposition of NCs (the ligand removal/exchange process for enhancing electronic coupling between NCs can be included as well prior to the post-treatment). From this project, we demonstrated that the LSPR properties or thermoelectric/electric properties of $Cu_{2-x}S$ NCs assemblies can be tuned using a chemical agent that either provides $Cu(I)^+$ to the

lattice (e.g., tetrakis copper hexafluorophosphate ($Cu(CH_3CN)_4PF_6$) or extracts $Cu(I)^+$ from the lattice (e.g., cerium ammonium nitrate ($(NH_4)_2Ce(NO_3)_6$). By changing the periods of time over which such chemical post-treatment was conducted, the physical properties of $Cu_{2-x}S$ NCs assemblies could be varied gradually. The results were reported in an article entitled "Stoichiometric Doping of Highly Coupled $Cu_{2-x}S$ Nanocrystal Assemblies" in ACS Appl. Mater. Interfaces 2021, 13, 26330. While the chemical method easily prepares a series of samples with gradually varied atomic stoichiometry that would be useful for systematic study, the method relying on reaction time control also fails to provide on-demand control on the atomic stoichiometry for $Cu_{2-x}S$ NCs with minimal batch-to-batch error.

Alternatively, we demonstrated the tuning of atomic stoichiometry for $Cu_{2-x}S$ NCs assemblies by exploiting heterocations (e.g., lithium ions and sodium ions) controlled by electrochemical methods. Electrochemical methods based on applied potential-dependent electrochemical reactions allows ion insertion/extraction reaction on $Cu_{2-x}S$ NCs assemblies to be reversibly controlled. We observe that the characteristic LSPR in NIR of $Cu_{2-x}S$ NCs assemblies can be suppressed based on electrochemical reaction induced at a negative potential applied to the assemblies, indicating that the density of hole carriers in the assemblies can be controlled. Meanwhile, the reversed reaction induced under a positive potential increased the hole density in the assemblies and amplified both the LSPR. The results were reported in an article entitled "Electrochemical Lithium Doping of $Cu_{2-x}S$ Nanocrystal Assemblies for Tuning Their Near Infrared Absorbance" in Journal of Mater. Chem. C 2023, 11, 4466.

$Cu_{2-x}S$ NCs used for this work were synthesized by a hot injection method described previously in the 1st year annual report (**Step 1**, **Figure 1a**). Copper (I) chloride and sulfur powder were used as copper and sulfur precursors, respectively. Oleylamine (OAm) was used as the reaction solvent as well as the ligands attached on the NC surface. The average diameter of the as-synthesized $Cu_{2-x}S$ NCs capped with OAm was 5.5 nm (inset in **Figure 1b**). The *x*-value of 0.9 was confirmed for these NCs based on composition analysis using X-ray photoemission spectroscopy (XPS). **Figure 1b** shows the UV-Vis-NIR spectrum of the resulting $Cu_{1.1}S$ NCs dispersed in trichloroethlene. The LSPR peak appearing at 1378 nm in the NIR regime indicates the plentiful of holes in $Cu_{1.1}S$ NCs created by the stoichiometry-dependent self-doping effect. The X-ray diffraction (XRD) pattern of the as-synthesized $Cu_{1.1}S$ NCs matches with that of covellite phase (CuS), consistent with previous results (**Figure 1c**). The $Cu_{2-x}S$ NCs were assembled onto a glass substrate coated with ITO contact by spin-coating (**Step 2**, **Figure 1d**). Morphology of the film observed using atomic force microscopy (AFM) is shown in **Figure 1e**. Despite the reduced average NC-NC distance in the assemblies (compared to that in solution), the thin-film also showed characteristic LSPR peak at 1124 nm in the NIR regime (**Figure 1f**).

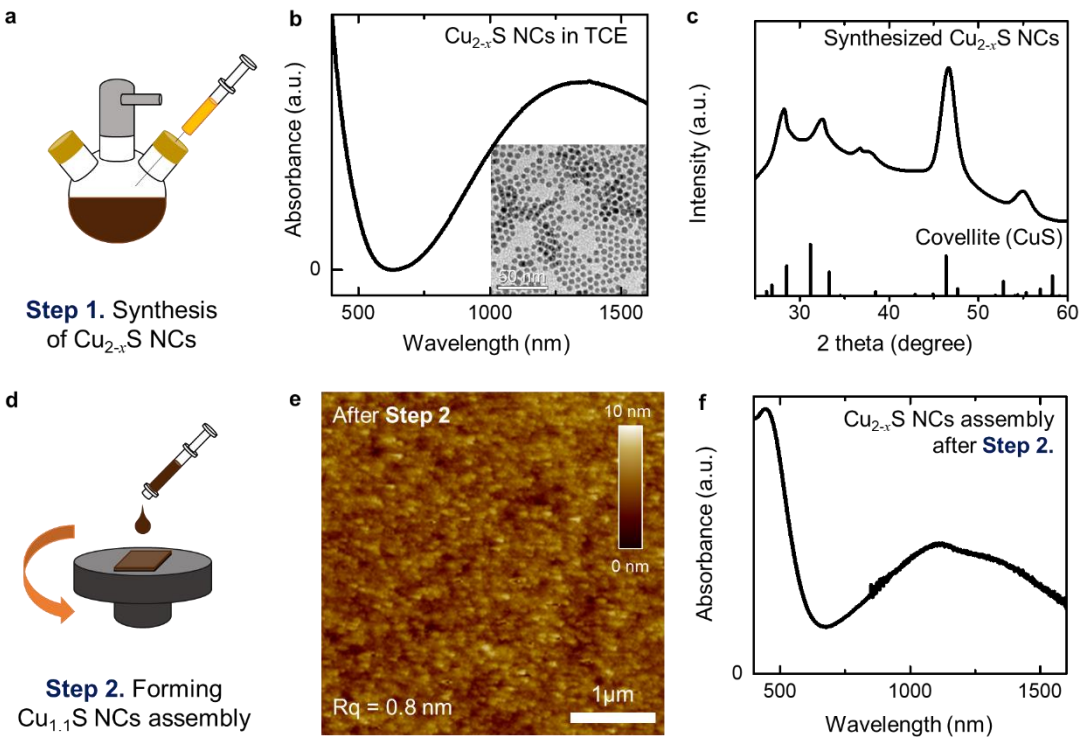

Figure 1. (a) Schematic for synthesis of $Cu_{2-x}S$ NCs (x = 0.9) synthesis (Step 1). (b) UV-Vis-NIR absorbance spectrum of the $Cu_{1.1}S$ NCs in solution (trichloroethylene). The inset is a TEM image of the $Cu_{1.1}S$ NCs. (c) X-ray diffractogram of $Cu_{1.1}S$ NCs. (d) Schematic for forming $Cu_{1.1}S$ NCs on ITO/glass substate (Step 2). (e) Atomic force microscope image of the resulting $Cu_{1.1}S$ NCs assembly. (f) UV-Vis-NIR absorbance spectrum of the $Cu_{1.1}S$ NCs assembly.

Subsequently, OAm ligands on the surface of $Cu_{1.1}S$ NCs were removed through Na_2S treatment (**Step 3**, **Figure 2a**). According to our previous report, dipping thin films of $Cu_{2-x}S$ NCs into a Na_2S solution in methanol completely removes OAm without altering the composition of $Cu_{2-x}S$ NCs. Dwelling (2 min) a drop of Na_2S solution (0.064 M in ethanol) onto the $Cu_{1.1}S$ NCs assemblies followed by spin-drying yielded the consist results. **Figure 2b** shows a series of Fourier-transform infrared (FT-IR) spectra for the $Cu_{2-x}S$ NCs assemblies before and after the Na_2S treatment step. The peak at around 2800-3000 cm^{-1} assigned to the stretching vibration of the C-H bond of oleylamine was completely negated after the Na_2S treatment step. The removal of insulating OAm from the surface of NCs not only enhanced electronic coupling between neighboring NCs and make the assemblies more conductive, but it also permitted easier access of ions (such as lithium ions or sodium ions) in electrochemical cells described below for electric potential-dependent electrochemical reactions. Because the ligand removal often produced

microscopic cracks in the film, we repeated the above spin-coating of NCs and ligand removal steps that were intended to fill the cracks while preserving good coupling between neighboring NCs. **Figure 2c** is the morphology of the resulting highly coupled $Cu_{1.1}S$ NCs assemblies observed using AFM. The RMS roughness of the film was 1.7 nm, indicating that repeated NC casting and ligand removal steps increases the surface roughness. UV-Vis-NIR absorbance spectrum of the resulting film is also shown in **Figure 2d**.

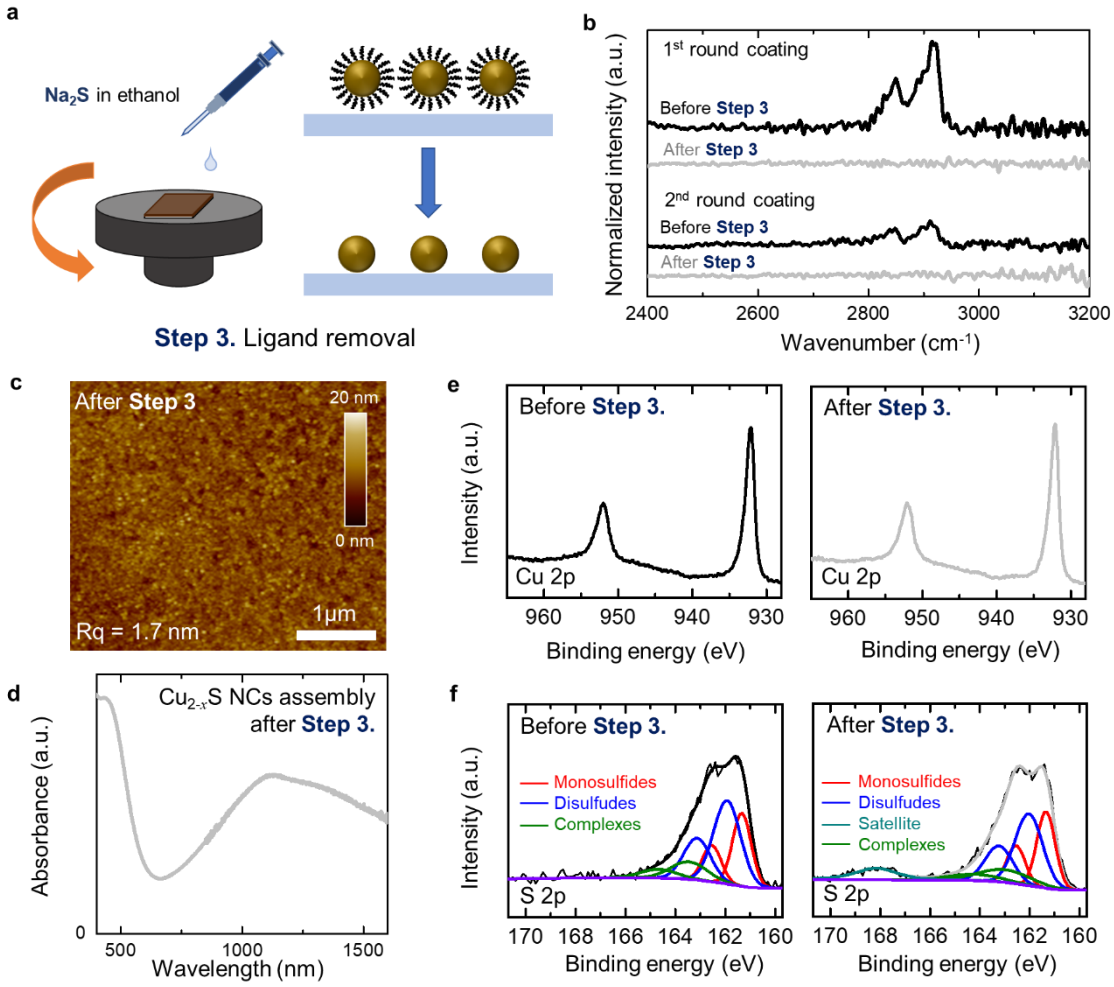

Figure 2 (a) Schematic for removing ligands on the $Cu_{1.1}S$ NCs assembly (Step 3). (b) Fourier transform infrared spectrum of $Cu_{1.1}S$ NCs assemblies at different stages in Step 3. (c). Atomic force microscope image of the $Cu_{1.1}S$ NCs assembly after Step 3. (d) UV-Vis-NIR absorbance spectrum of the $Cu_{1.1}S$ NCs assembly after Step 3. (e) High resolution Cu 2p XPS spectra for $Cu_{1.1}S$ NCs assembly before (left) and after (right) Step 3. (f) High resolution S 2p XPS spectra for $Cu_{1.1}S$ NCs assembly before (left) and after (right) Step 3. Deconvoluted subcomponents are colored for visualization.

We confirmed that the Na_2S treatment and the associated ligand removal did not alter the atomic composition of $Cu_{1.1}S$ NCs assemblies based on elemental analysis using XPS. Moreover, analysis of high-resolution XPS scans provided in depth understanding on the given samples. **Figure 2e** shows high-resolution XPS spectra for Cu 2p in $Cu_{1.1}S$ NCs assemblies before (left) and after (right) the Na_2S treatment. Two peaks at 932.1 and 952.0 eV were obtained, corresponding to Cu $2p_{3/2}$ and Cu $2p_{1/2}$, respectively, and no noticeably difference was observed between the samples. The results indicate that the oxidation state of copper element (i.e., +1) is not altered during the ligand removal step. **Figure 2f** shows high-resolution XPS spectra for S 2p in $Cu_{1.1}S$ NCs assemblies before (left) and after (right) the Na_2S treatment. As discussed above, the sulfur bonding in $Cu_{2-x}S$ NCs exists in two different forms; the monosulfide bonding (i.e., $[S^{2-}]$) and disulfide bonding (i.e., $[(S\text{-}S)^{-}]$). Considering the charge neutrality, this can be expressed in a chemical formula given as $Cu_{2-x}S = [Cu^{+}]_{2-x}[S^{2-}]_{1-2x/3}[(S\text{-}S)^{-}]_{x/3}$; for $Cu_{2-x}S$ NCs with $x = 0$ (i.e., $Cu_2S = [Cu^{+}]_2[S^{2-}]_1$) no sulfur forms disulfide boding, whereas for $Cu_{2-x}S$ NCs with $x = 1$, (i.e., $CuS = [Cu^{+}]_1[S^{2-}]_{0.33}[(S\text{-}S)^{-}]_{0.33}$), two third of sulfur contributes to form disulfide bonding. For our $Cu_{2-x}S$ NCs with $x = 0.9$, we expect the formula for $Cu_{1.1}S$ to be $[Cu^{+}]_{1.1}[S^{2-}]_{0.40}[(S\text{-}S)^{-}]_{0.30}$). The 0.40:0.30 ratio for $[S^{2-}]$:$[(S\text{-}S)^{-}]$ from this formula matches well with the areal ratio of the respective deconvoluted subcomponents of the S 2p XPS peak (the set of monosulfide peaks at 161.4 eV and 162.6 eV vs. the set of disulfide peaks at 162.1 eV and 163.3 eV) for our $Cu_{2-x}S$ NCs with $x = 0.9$ before (i.e, 0.41:0.30) and after (i.e, 58:42 =0.41:0.30) being treated with Na_2S.

Alternatively, the ligand treated $Cu_{2-x}S$ NCs ($x = 0.9$) assemblies prepared onto ITO served as the working electrode of an electrochemical cell that was prepared to conduct electric potential-controlled electrochemical reaction (e.g., lithiation) (**Figure 3a**). For the electrochemical cell, we employed a silver (pseudo) reference electrode and a platinum counter electrode. Propylene carbonate (PC) added with 100 mM of tetrabutylammonium perchlorate (TBAP) was used as the electrolyte. 100 mM of lithium perchlorate ($LiClO_4$) was added to the electrolyte which provided lithium ion for lithiation reaction at the working electrode (in the electrochemical cell for sodiation reaction, we instead added sodiaum perchlorate ($NaClO_4$) 1 mM of ferrocene (Fc) was also added to the electrolyte; the Fc/Fc^{+} couple served as the redox mediator to facilitate the lithiation (or sodiation) reaction at the working electrode. We emphasize that exploiting lithium ion in the electrochemical cell was critical for reversible control of atomic composition for the $Cu_{2-x}S$ NCs assemblies on the working electrode. Li^{+} is a monovalent cation. Therefore, the change in the lattice structure induced by Li^{+} insertion/extraction is expected to occur as it does by inserting/extracting $Cu(I)^{+}$ (for example by chemical treatment). Li^{+} is stable in its monovalent form in electrolytic environment and, therefore, it can be readily utilized in electrochemical cells. In contrast, Cu^{+} is like to undergo disproportion reaction in electrolytic environment ($2Cu^{+} \rightarrow Cu + Cu^{2+}$). Therefore, utilizing Cu^{+} in electrochemical cells requires meticulous control in the

electrolyte solution. In addition, the ionic radius for Li^+ is smaller than that of Cu^+. Therefore, the lattice of $Cu_{2-x}S$ NCs is less likely to be distorted upon multiple cycles of insertion and extraction. In fact, the storage/release of Li^+ on $Cu_{2-x}S$ NCs are under intensive investigation for the next-generation lithium ion-based energy storage devices.

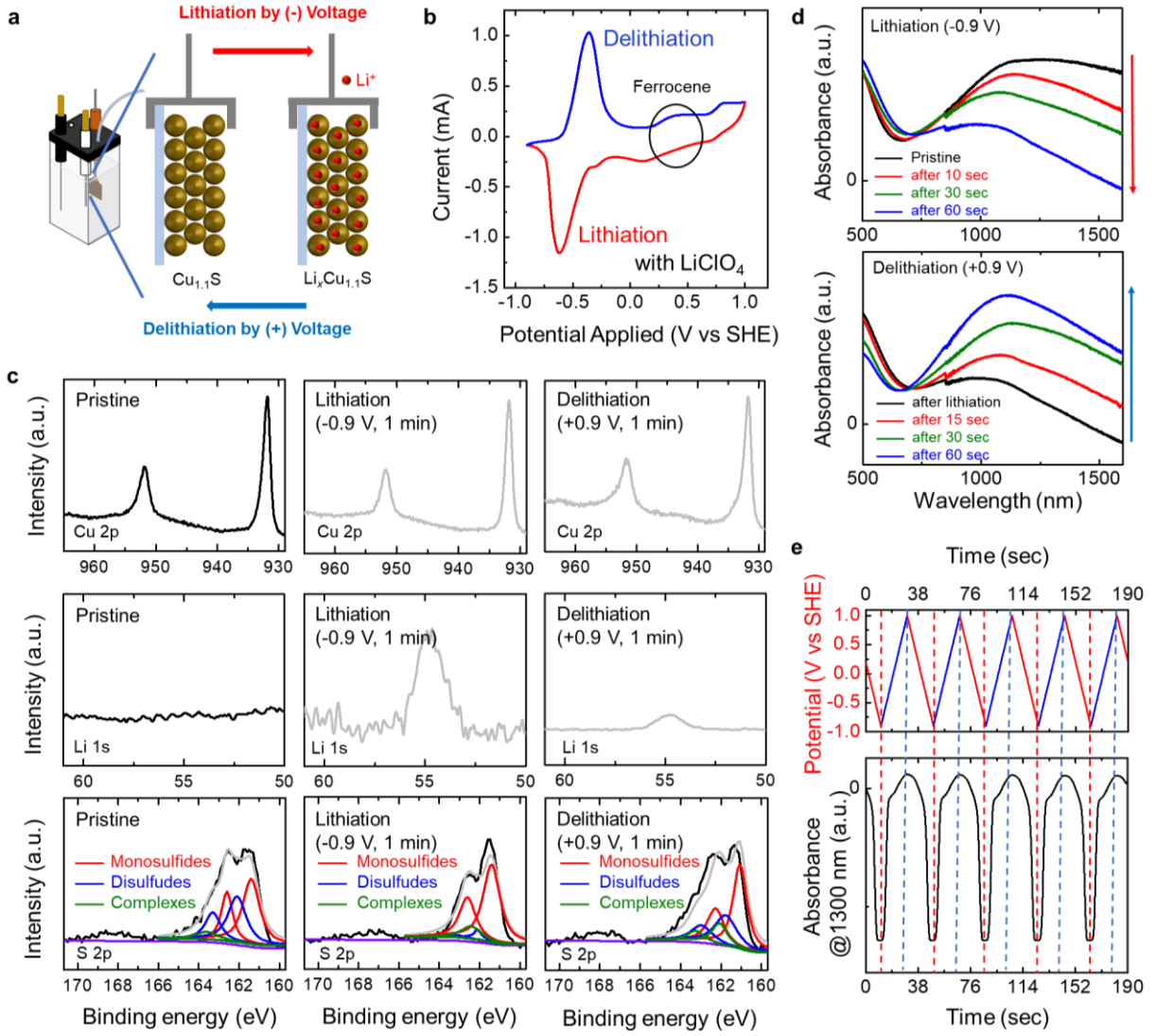

Figure 3 (a) Schematic for lithation/delithiation process for $Cu_{1.1}S$ NC assembly using electrochemical method. (b) Cyclic voltammogram for $Cu_{1.1}S$ NC assembly following lithation/delithiation process. (c) Sets of high-resolution Cu 2p (top row), Li 1s (middle row), and S 2p (bottom row) XPS spectra for $Cu_{1.1}S$ NCs assembly at different stages of lithiation and delithiation processes. (d) Evolution in the absorbance spectrum during lithiation (top) and delithiation proceeses. (e) Absorbance monitored at 1300 nm, while applying cycling voltages from -0.9 V and 1.0 V (scan rate = 100 mV/s).

Figure 3b displays a cyclic voltammogram of the given 3-electrode electrochemical cell. A sharp reduction peak was observed at -0.6 V (relative to SHE), which was reversibly coupled to the oxidation peak at -0.4 V. The small peak couple at +0.4 V is ascribed to the half-wave potential of Fc. We assign the reduction peak at -0.6 V in the forward scan to the lithiation reaction of $Cu_{1.1}S$ NCs, and the oxidation peak at -0.4 V in the reverse scan to the dilithiation reaction. When $Cu_{1.1}S$ NCs are lithiated, the sulfurs of disulfide bonding breaks to form metal-sulfur bondings (i.e., monosulfide bonds), akin to when additional $Cu(I)^+$ is introduced into the NCs. We can express this in a chemical equation given as yLi^+ (from electrolytic environment) + ye^- (from Fc/Fc^+ couple) + $Cu_{1.1}S$ (= $[Cu^+]_{1.1}[S^{2-}]_{0.40}[(S\text{-}S)^-]_{0.30}$) → $Li_yCu_{1.1}S$ (= $[Li^+]_y[Cu^+]_{1.1}[S^{2-}]_{0.40+2y/3}[(S\text{-}S)^-]_{0.30-y/3}$). Accordingly, we conjecture that the lithiation reaction induces transformation in the bonding characteristics of sulfur such that more monosulfide bondings are formed upon insertion of lithium ions. The transformation could be confirmed from the change in the shape of the S 2p XPS spectrum comprising subcomponents arising from monosulfides and disulfides. The top panel of **Figure 3c** shows the high resolution XPS scans of S 2p peaks for a $Cu_{1.1}S$ NCs assembly under different lithiation/delithiation conditions; the left panel shows the spectrum before applying any potential to the $Cu_{1.1}S$ NCs assembly (i.e, before lithiation), the middle panel shows results after applying -0.9 V (relative to SHE) for 1 min (the given lithiation condition yielded yielding $Li_{0.7}Cu_{1.1}S$ NCs of which the composition was determined from the XPS elemental analysis), and the right panel shows those after applying +0.9 V (relative to SHE) for 1 min to the already lithiated $Cu_{1.1}S$ NCs assembly (the given delithiation condition yielded yielding $Li_{0.1}Cu_{1.1}S$ NCs of which the composition was determined from the XPS elemental analysis). The areal ratio of the deconvoluted monosulide and disulfide subcomponents for the S 2p XPS peak was 58:42 (=0.41:0.30) before lithiation. This becomes 93:7 after the given lithiation condition, as the inserted lithium ions form breaks the disulfides and form monosulfide bondings. Finally, it becomes 67:33 after the given delithiation process. We note that the value does not recover its original value (i.e., 58:42). This is perhaps due to the residual lithium still contained in the NCs assembly even after the given dilithiation condition (yielding $Li_{0.1}Cu_{1.1}S$ NCs). The results are summarized in **Table 1**. The high-resolution scan of resolution XPS scans of Cu 2p (middle) and Li 1s (bottom) are also shown in the figure. Throughout the samples, the Cu-2p peaks appeared at 932.1 eV and 952.0 eV that are assigned to the binding energies of $2p_{3/2}$ and $2p_{1/2}$ of Cu^+, indicating that copper exists in +1 valency over the entire experiment. No sign of Li was observed from the as-prepared $Cu_{1.1}S$ NCs assembly, but after lithiation at -0.9 V (relative to SHE), Li-1s peak clearly appeared. This peak was reduced after the as-lithiated $Cu_{1.1}S$ NCs assembly was delithiated at +0.9 V (relative to SHE) but was not completely removed as discussed above. We note that even after application of the given delithiation potential over extended periods of time, the residual lithium component still appeared.

Table 1. Summary of chemical formula, degree of lithiation (y), and the areal ratio of the deconvoluted peaks of high-resolution S 2p spectra for of $Cu_{2-x}S$ NCs assemblies under different lithiation/delithiation conditions.

	Chemical Formula	y	Monosulfide (%)	Disulfide (%)	Complexes (%)
Pristine	$Cu_{1.1}S$	0	49	36	15
Lithiation (-0.9 V, 1 min)	$Li_{0.7}Cu_{1.1}S$	0.7	76	6	15
Delithiation (+0.9 V, 1 min)	$Li_{0.1}Cu_{1.1}S$	0.1	54	31	15

The lithiation process leading to change in the characteristics of sulfur bonding is also expected to change the hole density of the $Cu_{1.1}S$ NCs assembly, similar to what was done after inserting additional $Cu(I)^+$ from chemical methods. The UV-Vis-NIR absorbance of the $Cu_{1.1}S$ NCs assemblies was monitored while applying a potential to the assemblies using a spectroelectrochemistry setup. As introduced above, the characteristic NIR absorbance of $Cu_{1.1}S$ NCs assemblies is attribute to LSPR, of which the peak intensity is a sensitive function of hole density of the materials. When a potential more negative than the peak reduction potential from **Figure 3b** (i.e., -0.6 V relative to SHE) was applied (e.g. -0.9 V) to an as-prepared $Cu_{1.1}S$ NCs assembly, the LSPR absorbance of the peak gradually decreased with time, indicating its hole density is lowered (**Figure 3d**). When a potential more positive than the peak oxidation potential in the reverse scan of the cyclicvoltamogram (-0.6 V relative to SHE) was applied (e.g. +0.9 V) was applied to this lithiated $Cu_{1.1}S$ NCs assembly, the absorbance peak in NIR gradually increased, indicating that its hole density is recovered (**Figure 3e**). The lithiation and delithiation processes and the associated change in LSPR were reversible and could be repeated multiple times (despite the residual amount of lithium remained in the lattice even after the given delithiation conditions). **Figure 3f** shows variation in the NIR absorbance at 1300 nm that was monitored upon sweeping the potential applied to the $Cu_{1.1}S$ NCs assembly in cycles (same as what was done for cyclic voltammetry).

We note that by including $NaClO_4$ in the electrochemical cell instead of $LiClO_4$, the $Cu_{1.1}S$ NCs assembly could be sodiated electrochemically as well (**Figure 4a**). Sodiation/desodiation of $Cu_{2-x}S$ is also well-exploited in energy storage applications. Cyclic voltammogram of the electrochemical cell containing instead of $NaClO_4$ is shown in **Figure 4b**. A sharp reduction peak was observed at -0.5 V (relative to SHE), which was reversibly coupled to the oxidation peak at -0.9 V. The small peak couple at +0.4 V is ascribed to the half-wave potential of Fc. **Figure 4c** shows a series of UV-Vis-NIR spectra that was recorded upon applying a potential sufficiently negative to yield sodiation reaction. The absorbance in NIR based on LSPR gradually reduced

upon applying the potential over time. This absorbance was recovered gradually when a potential sufficiently positive to yield desodiation of the sodiated $Cu_{1.1}S$ NCs assembly was applied. Consistent with **Figure 3f** for lithiation/delithiation, sweeping the potential applied to the $Cu_{1.1}S$ NCs assembly in cycles (same as what was done for cyclic voltammetry) yielded reversible variation in the NIR absorbance at 1300 nm (**Figure 4d**). Unlike the as-lithiated/delithiated $Cu_{1.1}S$ NCs assemblies, however, the sodiated $Cu_{1.1}S$ NCs assemblies were poorly stable under ambient condition. Therefore, the entire cyclic voltammetry and spectroelectrochemical analysis of these samples had to be conducted under nitrogen condition. (brief exposure to ambient yielded completely different, on-reproducible data). XPS analysis or XRD analysis on the sodiated/desodiated samples could not be carried out (which inevitably requires short exposure to ambient during the analysis/loading).

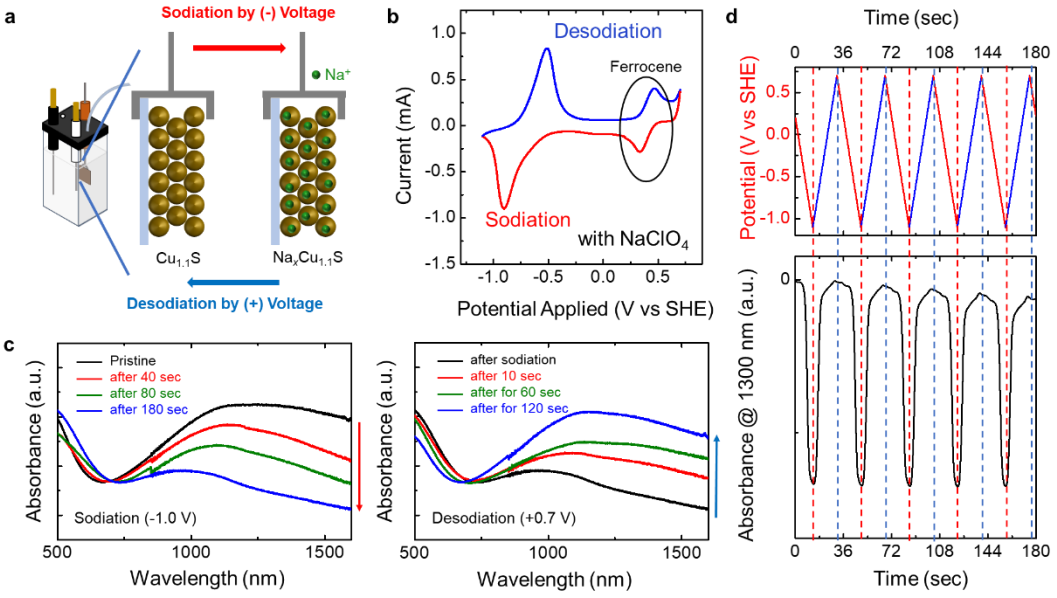

Figure 4 (a) Schematic for sodiation/desodiation process for $Cu_{1.1}S$ NC assembly using electrochemical method. (b) Cyclic voltammogram for $Cu_{1.1}S$ NC assembly following sodiation/desodiation process. (c) Evolution in the absorbance spectrum during sodiation (left) and delithiation (right) proceeses. (d) Absorbance monitored at 1300 nm, while applying cycling voltages from -0.7 V and 1.1 V (scan rate = 100 mV/s).

REFERENCES

C. Coughlan, M. Ibanez, O. Dobrozhan, A. Singh, A. Cabot and K. M. Ryan, Chem. Rev., 2017, 117, 5865-6109.

J. M. Luther, P. K. Jain, T. Ewers and A. P. Alivisatos, Nat. Mater., 2011, 10, 361-366.

X. Liu, X. Wang, B. Zhou, W. C. Law, A. N. Cartwright and M. T. Swihart, Adv. Funct. Mater., 2013, 23, 1256-1264.

Y. Xie, A. Riedinger, M. Prato, A. Casu, A. Genovese, P. Guardia, S. Sottini, C. Sangregorio, K. Miszta, S. Ghosh, T. Pellegrino and L. Manna, J. Am. Chem. Soc., 2013, 135, 17630-17637.

T. A. Patel and E. Panda, Appl. Surf. Sci., 2019, 488, 477-484.

Y. He, T. Day, T. Zhang, H. Liu, X. Shi, L. Chen and G. J. Snyder, Adv. Mater., 2014, 26, 3974-3978.

G. Kalimuldina, A. Nurpeissova, A. Adylkhanova, D. Adair, I. Taniguchi and Z. Bakenov, ACS Appl. Energy Mater., 2020, 3, 11480-11499.

Y. Wu, C. Wadia, W. Ma, B. Sadtler and A. P. Alivisatos, Nano Lett., 2008, 8, 2551-2555.

M. Basu, A. K. Sinha, M. Pradhan, S. Sarkar, Y. Negishi and T. Pal, Environ. Sci. Technol., 2010, 44, 6313-6318.

C.-H. Lai, K.-W. Huang, J.-H. Cheng, C.-Y. Lee, B.-J. Hwang and L.-J. Chen, J. Mater. Chem., 2010, 20, 6638-6645.

A. Šetkus, A. Galdikas, A. Mironas, I. Šimkiene, I. Ancutiene, V. Janickis, S. Kaciulis, G. Mattogno and G. Ingo, Thin Solid Films, 2001, 391, 275-281.

M. Li, Y. Liu, Y. Zhang, X. Han, T. Zhang, Y. Zuo, C. Xie, K. Xiao, J. Arbiol and J. Llorca, ACS Nano, 2021, 15, 4967-4978.

B. Jache, B. Mogwitz, F. Klein and P. Adelhelm, J. Power Sources, 2014, 247, 703-711.

G. Kalimuldina and I. Taniguchi, J. Power Sources, 2016, 331, 258-266.

K. Jiang, Z. Chen and X. Meng, ChemElectroChem, 2019, 6, 2825-2840.

J.-S. Chung and H.-J. Sohn, J. Power Sources, 2002, 108, 226-231.

H. Wu, T. Li, H. Li, D. Zhang and F. Xu, Mater. Lett., 2020, 262, 127181.

W. Lou, M. Chen, X. Wang and W. Liu, J. Phys. Chem. C, 2007, 111, 9658-9663.

O. Elimelech, J. Liu, A. M. Plonka, A. I. Frenkel and U. Banin, Angew. Chem., 2017, 129, 10471-10476.

A. T. Sheardy, D. M. Arvapalli and J. Wei, Nanoscale Adv., 2020, 2, 1054-1058.

S. Gorai, D. Ganguli and S. Chaudhuri, Cryst. Growth Des., 2005, 5, 875-877.

S. Yadav, K. Shrivas and P. Bajpai, J. Alloys Compd, 2019, 772, 579-592.

S. Yadav and P. Bajpai, Nano-Struct. Nano-Objects, 2017, 10, 151-158.

C. H. Van Oversteeg, F. E. Oropeza, J. P. Hofmann, E. J. Hensen, P. E. De Jongh and C. de Mello Donega, Chem. Mater., 2018, 31, 541-552.

J. Li, T. Jiu, G.-H. Tao, G. Wang, C. Sun, P. Li, J. Fang and L. He, J. Colloid Interface Sci., 2014, 419, 142-147.

M. Jain, D. G. Babar and S. S. Garje, Appl. Nanosci., 2019, 9, 353-367.

L. Liu, B. Zhou, L. Deng, W. Fu, J. Zhang, M. Wu, W. Zhang, B. Zou and H. Zhong, J. Phys. Chem. C, 2014, 118, 26964-26972.

M. Lee, J. Yang, H. Lee, J. I. Lee, A. R. Koirala, J. Park, H. Jo, S. Kim, H. Park and J. Kwak, ACS Appl. Mater. Interfaces, 2021, 13, 26330-26338.

Y. Zhao, H. Pan, Y. Lou, X. Qiu, J. Zhu and C. Burda, J. Am. Chem. Soc., 2009, 131, 4253-4261.

J. M. Luther, M. Law, Q. Song, C. L. Perkins, M. C. Beard and A. J. Nozik, ACS Nano, 2008, 2, 271-280.

H. Zhang, J. Jang, W. Liu and D. V. Talapin, ACS Nano, 2014, 8, 7359-7369.

J. Lee, Y. Gim, J. Yang, H. Jo, J. Han, H. Lee, D. H. Kim, W. Huh, J. H. Cho and M. S. Kang, J. Phys. Chem. C, 2017, 121, 5436-5443.

A. Nag, M. V. Kovalenko, J.-S. Lee, W. Liu, B. Spokoyny and D. V. Talapin, J. Am. Chem. Soc., 2011, 133, 10612-10620.

N. Y. Shim, D. A. Bernards, D. J. Macaya, J. A. DeFranco, M. Nikolou, R. M. Owens and G. G. Malliaras, Sens., 2009, 9, 9896-9902.

S. Dong, B. Wang and B. Liu, Biosens. Bioelectron, 1992, 7, 215-222.

J. Kardos, L. Héja, Á. Simon, I. Jablonkai, R. Kovács and K. Jemnitz, Cell Commun. Signal., 2018, 16, 1-22.

J. Brugger, B. Etschmann, W. Liu, D. Testemale, J.-L. Hazemann, H. Emerich, W. Van Beek and O. Proux, Geochim. Cosmochim. Acta, 2007, 71, 4920-4941.

K. Shakeela, A. S. Dithya, C. J. Rao and G. R. Rao, J. Chem. Sci., 2015, 127, 133-140.

D. Shen, K. Steinberg and R. Akolkar, J. Electrochem. Soc., 2018, 165, E808.

K. He, Z. Yao, S. Hwang, N. Li, K. Sun, H. Gan, Y. Du, H. Zhang, C. Wolverton and D. Su, Nano Lett., 2017, 17, 5726-5733.

J. S. Nam, J.-H. Lee, S. M. Hwang and Y.-J. Kim, J. Mater. Chem. A, 2019, 7, 11699-11708.

R. R. Gagne, C. A. Koval and G. C. Lisensky, Inorg, 1980, 19, 2854-2855.

H. Singh, S. Kumar and P. K. Sharma, Appl. Surf. Sci., 2023, 612, 155831.